



A Journal of the Gesellschaft Deutscher Chemiker

Angewandte Chemie

GDCh

International Edition

www.angewandte.org

Accepted Article

Title: Molecular Vise Approach to Create Metal-Binding Sites in MOFs and Detection of Biomarker

Authors: Yang Wang, Qi Liu, Qin Zhang, Bosi Peng, and Hexiang Deng

This manuscript has been accepted after peer review and appears as an Accepted Article online prior to editing, proofing, and formal publication of the final Version of Record (VoR). This work is currently citable by using the Digital Object Identifier (DOI) given below. The VoR will be published online in Early View as soon as possible and may be different to this Accepted Article as a result of editing. Readers should obtain the VoR from the journal website shown below when it is published to ensure accuracy of information. The authors are responsible for the content of this Accepted Article.

To be cited as: *Angew. Chem. Int. Ed.* 10.1002/anie.201803201
Angew. Chem. 10.1002/ange.201803201

Link to VoR: <http://dx.doi.org/10.1002/anie.201803201>
<http://dx.doi.org/10.1002/ange.201803201>

Molecular Vise Approach to Create Metal-Binding Sites in MOFs and Detection of Biomarker

Yang Wang[†], Qi Liu[†], Qin Zhang, Bosi Peng, and Hexiang Deng^{*}

Abstract: We report a new approach to create metal-binding site in a series of metal-organic frameworks (MOFs), where tetra-topic carboxylate linker, 4',4'',4''',4''''-methanetetrayltetrabiphenyl-4-carboxylic acid, is partially replaced by a tri-topic carboxylate linker, tris(4-carboxybiphenyl)amine, in combination with mono-topic linkers, formic acid, trifluoroacetic acid, benzoic acid, isonicotinic acid, 4-chlorobenzoic acid, and 4-nitrobenzoic acid, respectively. The distance between these paired-up linkers can be precisely controlled, ranging from 5.4 to 10.8 Å, where a variety of metals, Mg²⁺, Al³⁺, Cr³⁺, Mn²⁺, Fe³⁺, Co²⁺, Ni²⁺, Cu²⁺, Zn²⁺, Ag⁺, Cd²⁺ and Pb²⁺, can be placed in. The distribution of these metal-binding sites across a single crystal is visualized by 3D tomography of laser scanning confocal microscopy with a resolution of 10 nm. The binding affinity between the metal and its binding-site in MOF can be varied in a large range (observed binding constants, K_{obs} from 1.56×10^2 to 1.70×10^4 Lmol⁻¹), in aqueous solution. The fluorescence of these crystals can be used to detect biomarkers, such as cysteine, homocysteine and glutathione, with ultra-high sensitivity and without the interference of urine, through the dissociation of metal ions from their binding sites.

Introduction of additional metal ions (metalation) into the pores of metal-organic frameworks (MOFs) has been done through (1) substitution of metal ions within, or addition to the multi-metallic secondary building units (SBUs),¹ and (2) chelation of metals either directly to the organic strut of backbone or to a dangling functionality.² This metallation chemistry has led to enhancement in capacity and selectivity of gases uptake, and better catalytic performance, due to the specific interaction between the metal-binding site and guest molecules. Herein, we introduce a third metallation strategy, where metals are placed in between a pair of rigid linkers precisely anchored in opposite position within MOF crystal lattice like a vise (Figure 1A). One end of the vise is stationary and unchanged; while the other end can be altered to vary the distance between the two parts, thus precisely control the metal-binding site. In this study, we demonstrated this “molecular vise (MV) approach” in PCN-521,³ a MOF constructed from tetra-topic organic linkers (4',4'',4''',4''''-methanetetrayltetrabiphenyl-4-carboxylic acid, MTBC) and octa-topic second building units (SBUs, Figure S34, Supporting Infor-

mation, SI). The original tetra-topic linker was partially replaced by a pair of tri-topic linker, tris(4-carboxybiphenyl)amine (TBPA) and a mono-topic linker, likened to the stationary jaw and sliding jaw of the molecular vise, respectively, and form the corresponding MV-MOF (MV-PCN-521-R, R represents the mono-topic linker). Six different mono-topic linkers (formic acid, FA; trifluoroacetic acid, TFA, benzoic acid, BA; isonicotinic acid, IA; 4-chlorobenzoic acid, CBA, and 4-nitrobenzoic acid, NBA) with different functionality were used to form six MV-MOFs (MV-PCN-521-FA, -TFA, -BA, -IA, -CBA, -NBA, respectively, Figure 1C), each of which provides a unique space and chemical environment to bind with metal ions (Mg²⁺, Al³⁺, Cr³⁺, Mn²⁺, Fe³⁺, Co²⁺, Ni²⁺, Cu²⁺, Zn²⁺, Ag⁺, Cd²⁺ and Pb²⁺). The distribution of these metal-binding sites across a single crystal can be directly visualized, for the first time, by super resolution laser scanning confocal microscopy (SR-LSCM) with 10 nm accuracy. Furthermore, we show that one of these MV-MOFs in nanoscale, nano-MV-PCN-521-IA can bind with Cu²⁺ to quench the fluorescence of its nanocrystals, and function as a switch-on sensor to precisely detect the concentration of biomarkers, such as L-cysteine (Cys) in urine, with extremely low detection limit of 22.5 nM.

Fine tuning of coordination environment for metals has been a major theme in the development of coordination chemistry, however, this usually accompanied with changes in the geometry of ligands around the metal. In this study, when the tri-topic and mono-topic linkers were introduced into MOF lattice in pairs by MV approach, their relative position and geometry were fixed. This unique construct allowed us to systematically vary the coordination environment for metal without altering the geometry of ligands. In this way, the binding affinity between the metal and its binding-site in MOF can be varied with hundred-fold difference in aqueous solution, which hasn't been observed in any previous studies.

In the typical synthesis of MV-MOFs, MV-PCN-521 for example, MTBC, TBPA and mono-topic linkers with different functional groups were mixed with ZrCl₄ to form a clear solution in N, N-diethylformamide at 120 °C. This solution was kept in oven for 3 days to yield transparent octahedral shaped MV-PCN-521 crystals with the size about 100 μm (Figure 2A, Section S2, SI), when the ratio of TBPA/MTBC was less than 4:1 in the starting material. If more TBPA was used, another kind of crystals with hexagonal prism shape emerged, representing a new MOF with 2D structure in space group *Cmca*, here we named WHU-105 (Figure S24 and Table S6, SI). Detailed phase diagram for the synthesis of pure WHU-105 and MV-PCN-521 was illustrated in Figure S25 in SI. Powder X-ray diffraction (PXRD) patterns of MV-PCN-521 revealed that the underlying topology of the parent MOF, PCN-521, was preserved (Figure S21, S22 and S27, SI). From the single crystal X-ray diffraction (SC-XRD) experiments, both PCN-521 and MV-PCN-521 crystals synthesized in this study exhibited higher symmetry in

[*] Y. Wang[†], Dr. Q. Liu[†], Q. Zhang, B. Peng, and Prof. H. Deng
Key Laboratory of Biomedical Polymers-Ministry of Education, College of Chemistry and Molecular Sciences, Wuhan University
Wuhan 430072 (PR China)
E-mail: hdeng@whu.edu.cn
Dr. Q. Liu, and Prof. H. Deng
UC Berkeley-Wuhan University Joint Innovative Center, The Institute of Advanced Studies, Wuhan University
Wuhan 430072 (PR China)

[†] These authors contributed equally to this work.

Supporting information for this article is given via a link at the end of the document.

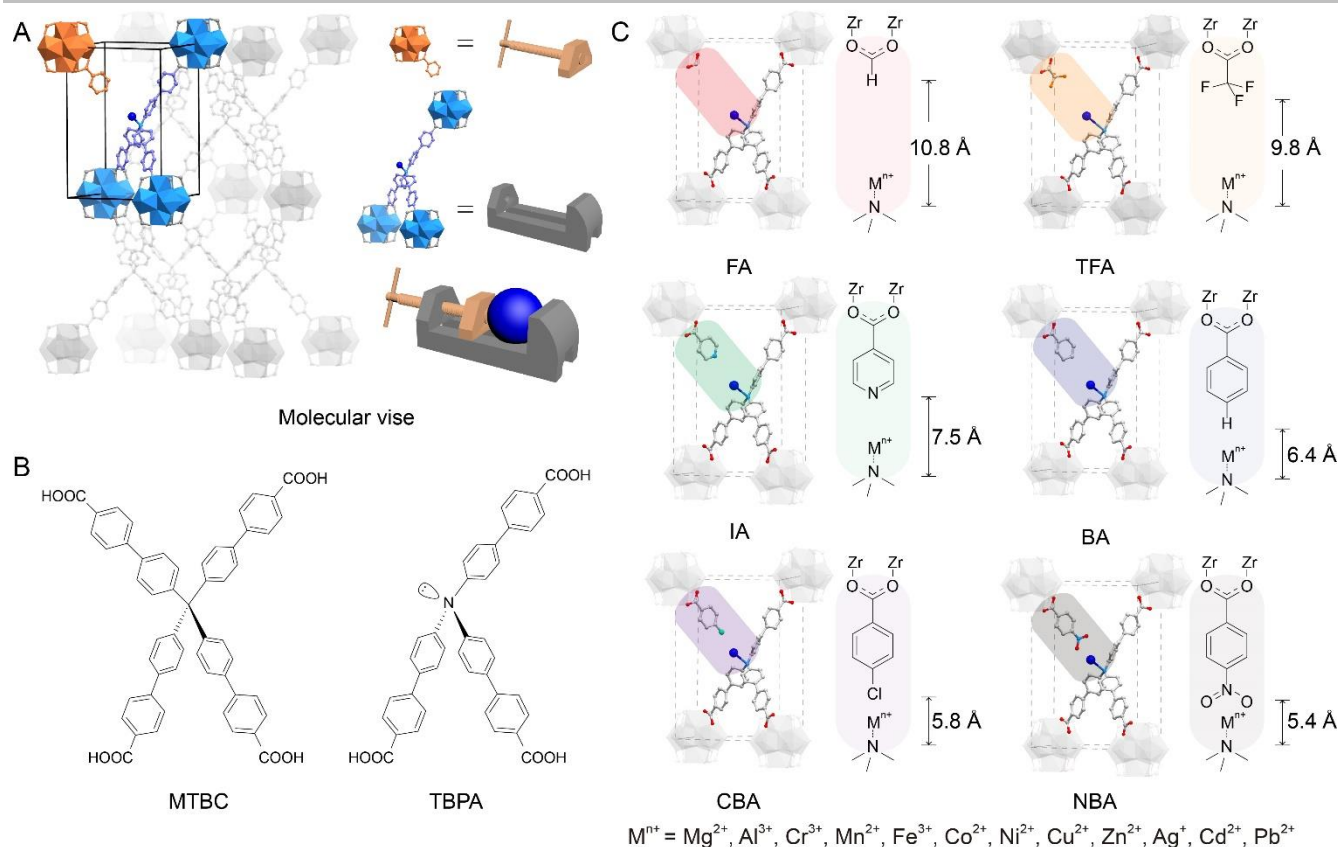


Figure 1. (A) Illustration of MV-MOF created by molecular vise approach. (B) Organic linkers used to construct MV-PCN-521. (C) Different metal-binding sites created by various mono-topic linkers.

space group $I4/mmm$ in comparison to previous reports. A slightly different unit cell was observed as the original tetra-topic linker, MTBC, was partially replaced by a pair of tri-topic linker, TBPA and mono-topic linker, BA, in MV-PCN-521-BA_{0.1} (0.1 here represents the molar ratio of TBPA in MOF crystal). Specifically, longer *c* axis [41.459(3) Å] and shorter *a* axis [20.3794(14) Å] were observed in this MV-MOF in comparison to the parent PCN-521 structure [*a* = 21.0704(9) Å, *c* = 40.3672(17) Å]. The replacement of MTBC by TBPA and mono-topic linkers requires them to fit into the original tetrahedron geometry of MTBC. There were two different angles between the phenyl units of TBPA, 105.9° and 117.0°, revealing in the crystal structure of MV-PCN-521-BA_{0.1}, both fell well into the possible bending range of tri-phenyl-amine type of organic linkers (105.5° to 129.3°) according to crystal structures in Cambridge Structural Database. The full coordination of all three carboxyl groups of TBPA and that of mono-topic linker with Zr₆O₈ SBUs was further demonstrated by ¹³C solid-state nuclear magnetic resonance (SSNMR), where 168.0 ppm peak in the spectra of the pure organic linkers was completely shifted to 171.0 ppm in spectra of MV-PCN-521-BA_{0.1} (Figure S65 and S66, SI). The opposition arrangement between mono-topic linker and tri-topic linker was confirmed by the absence of residual electron density around the coordinated water of SBU in the difference electron density map of MV-PCN-521-BA_{0.1} (Figure S33, SI). Nano-crystals of these MV-MOFs, termed as nano-MV-PCN-521-R here (Section S2.2, SI), were also synthesized, by applying vigorous stirring in the reaction solution, instead of stationary placement. Different from MV-PCN-521 crystals with 100 μm size, a larger portion of TBPA can be introduced into these nano-crystals, without sacrificing phase purity.

The co-existence of TBPA and MTBC linkers in MV-PCN-521 crystals of both micrometer and nanometer sizes was confirmed by the presence of TBPA signals (132.8 ppm) in ¹³C SSNMR spectra (Figure S65 and S66, SI). The precise ratio of tri-topic linker was determined by the ¹H NMR of digested MV-PCN-521 samples with the fingerprint chemical shift of 7.20-7.25 ppm. Integration of the peak intensities revealed that the presence of TBPA in MV-PCN-521-BA_{0.1} was 11% (Figure S67, SI). In contrast, more than 50% of TBPA can be introduced into nano-MV-PCN-521 (Figure S68 to S71, SI). Structural simulation of these nano-crystals showed that the integrity of the frameworks can be maintained by replacing two out of four MTBC linkers with TBPA linkers in one unit cell (Figure S37 to S42, SI). Scanning electron microscopy (SEM) images revealed that the shape of nano-MV-PCN-521 crystals changed from octahedral to truncated cube (Figure 2I, S72 and S73, SI). It was worth noting that the ratio of mono-topic linker to tri-topic TBPA linker was determined to be always 1:1 by ¹H NMR of digested MV-PCN-521 samples, no matter how much of TBPA was introduced into MV-MOF backbone (Table S1). This combined with the unaltered underlying topology of the parent MOF in crystallographic studies demonstrated the pair-up nature of mono-topic linker and tri-topic linker in MV-MOF-PCN-521 crystals (Figure 1C, S29-S31, SI). This allowed us to simulate the opposite arrangement of these linker pairs in MV-MOFs, from which the distance between Nitrogen atom of TBPA and the terminal functional group of the mono-topic linker was determined (Figure 1C, and S36 to S48, SI).

The permanent porosity of these MV-MOFs was assessed by N₂ adsorption at 77 K. Type-I curves were observed in their isotherms and the calculated Brunauer-Emmett-Teller (BET)

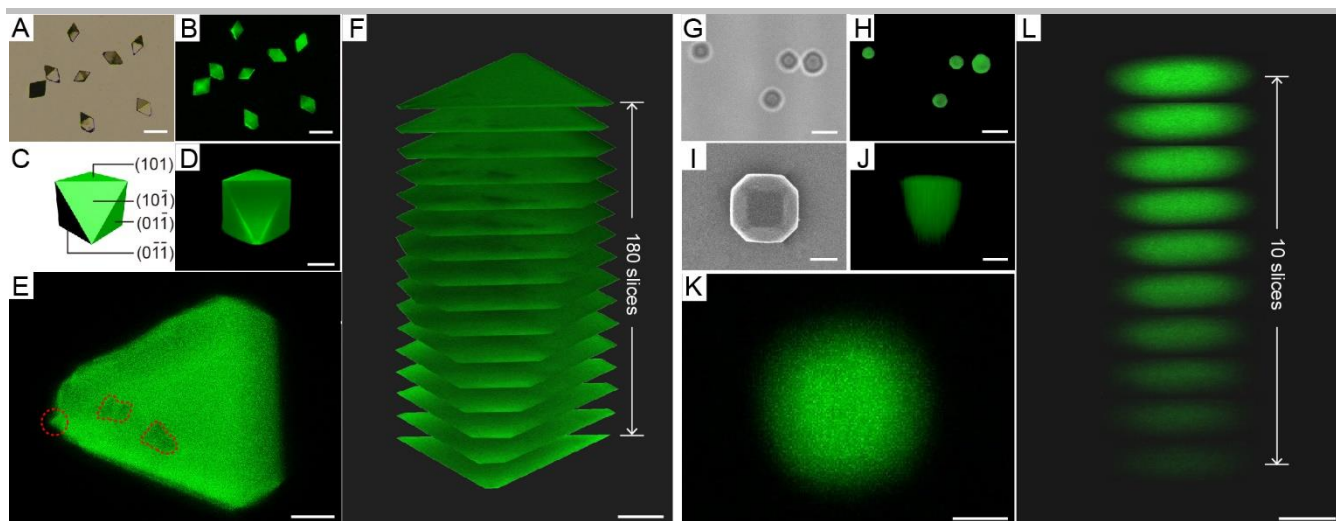


Figure 2. 3D tomography of both MV-PCN-BA_{0.1} (A-F) and nano-MV-PCN-521-BA (G-L) by laser scanning confocal microscopy. (A) Bright field image, and (B) LSCM image, scale bar 100 μm , (C) Model of octahedral crystal of MV-MOF, (D) 3D reconstruction of MV-MOF in 100 μm size, scale bar 20 μm . (E) One slice of (F) consecutive LSCM sections of MV-MOF, scale bar 20 μm . (G) Bright field image, and (H) STED image, scale bar 1 μm . (I) SEM image, and (J) 3D reconstruction of nano-MV-MOF, scale bar 500 nm. (K) One slice of (L) consecutive LSCM sections of nano-MV-MOF, scale bar 500 nm. Region of twin crystal and bubbles in MV-MOF (E) was highlighted in red dashes.

surface areas were 4000, 3390, 3320 m^2g^{-1} for MV-PCN-521-BA_{0.1}, MV-PCN-521-BA_{0.05} and PCN-521, respectively (Figure S51 to S56, SI), where the surface areas of MV-MOFs were higher than that of the parent MOF. Based on these observations, partial linker replacement in MOF structure was indeed an efficient way to increase inner surface, in good accordance with previous studies.⁴ However, when too much replacement occurred, as illustrated here by nano-MV-PCN-521 crystals with higher percentage (more than 50%) of TBPA, slightly lower surface areas were observed, ranging from 1980 to 3090 m^2g^{-1} . These MV-PCN-521 exhibited high chemical stability, evidenced by unaltered sharp peaks in their PXRD patterns after immersion in water for 6 days (Figure S50, SI). Thermogravimetric analysis (TGA) of these MV-MOFs showed no weight loss until 550 $^{\circ}\text{C}$ in air (Figure S78 to S81, SI).

Introduction of multiple functional groups into MOF structure has attracted a lot of attentions in recent MOF studies due to the synergy of these components and the flexibility in tuning pore environments without altering the target topology.⁵ One of the remaining challenges was to decipher the spatial arrangement of these functional components.⁶ Similarly, the distribution of TBPA and mono-topic linkers in MV-PCN-521 was hard to determine using XRD measurement due to both occupational and displacement disorder. In this study, given the fluorescence of TBPA linkers, we applied laser scanning confocal microscopy (LSCM)⁷ to detect the distribution of TBPA linker throughout the crystals of MV-MOFs (Figure 2). Green fluorescence was clearly observed in all the MV-PCN-521 crystals examined under excitation light of 405 nm, indicating the successful replacement of TBPA with MTBC, while PCN-521 exhibits no fluorescence under the same condition (Figure 2A, 2B and S74 to 76, SI).

The precise distribution of metal-binding site in MV-MOF single crystal was mapped layer by layer using fluorescence of TBPA linker through three-dimensional (3D) tomography. An octahedral single crystal with the edge of 92 μm was examined along [101] direction by 180 slices, from which a 3D reconstruction of the crystal was generated, in good accordance with the 3D model (Figure 2C and 2D). The thickness of each slice is about 90 nm, and the resolution within the slice is about 180 nm according to the limit by the wavelength of the incident

light [$\lambda=405\text{ nm}$, $d = \lambda/(2NA)$],⁸ corresponding to 45 and 65 unit cells along and perpendicular to [101] direction, respectively (Figure 2E and 2F). 56 slices from top to bottom with equal space were displayed in Figure S74, where metal-binding sites distributed all over these slices. Due to the high resolution of LSCM, we were able to observe every structural details of the crystal such as tiny bubbles and small twin crystal regions within the whole MV-MOF crystal (Figure 2E). Here, the sizes of the bubble and twin crystal circled in red dashes were 15 and 7 μm , respectively. More than three MV-PCN-521 crystals in 100 μm sizes were examined, where similar phenomena could be observed, since no perfect crystal exists (Figure S74 to S76, SI).

In comparison to crystals of 100 μm size, the distribution of metal-binding sites in nano-MV-PCN-521 crystals was more homogeneous, reflected on their LSCM and stimulated emission depletion (STED) images (Figure 2H, 2J, 2L, 2K and S77). One truncated cube crystal with the size of around 800 nm was examined by 3D tomography with 10 slices, each of which provides a fluorescence map of 10 nm resolution within the slice, corresponding to 5 unit cells. Note that the resolution along the excitation light was slightly sacrificed to guarantee the resolution in the focal plane.

The coordination between metals and metal-binding sites in MV-MOF crystals can be directly visualized by the instantaneous fluorescence quench of these crystals, once in contact with aqueous solutions of metal salt (Figure 3A). This is triggered by ligand-metal charge transfer (LMCT) between the tertiary amine TBPA linker and the metal cations at the metal-binding site.⁹ These metals can be readily removed from the metal-binding sites in MV-MOFs, when stronger coordinating ligands was added in, thus leading to the recovery of fluorescence. A large variety of metals, Mg^{2+} , Al^{3+} , Zn^{2+} , Cr^{3+} , Mn^{2+} , Fe^{3+} , Co^{2+} , Ni^{2+} , Cu^{2+} , Ag^{+} , Cd^{2+} and Pb^{2+} , can be placed at the metal-binding sites in these MV-MOFs created by molecular wise approach (Figure S84 to S108, SI). Quantitative binding and dissociation of metals were observed, regardless of the space and functionalities within these metal binding sites. This was evidenced in the peak shift of metals and N in the linkers in their X-ray photoelectron spectroscopy (XPS) spectra (Figure 3B to 3E). Specifically, in the case of nano-MV-PCN-521-FA, Cu^{2+}

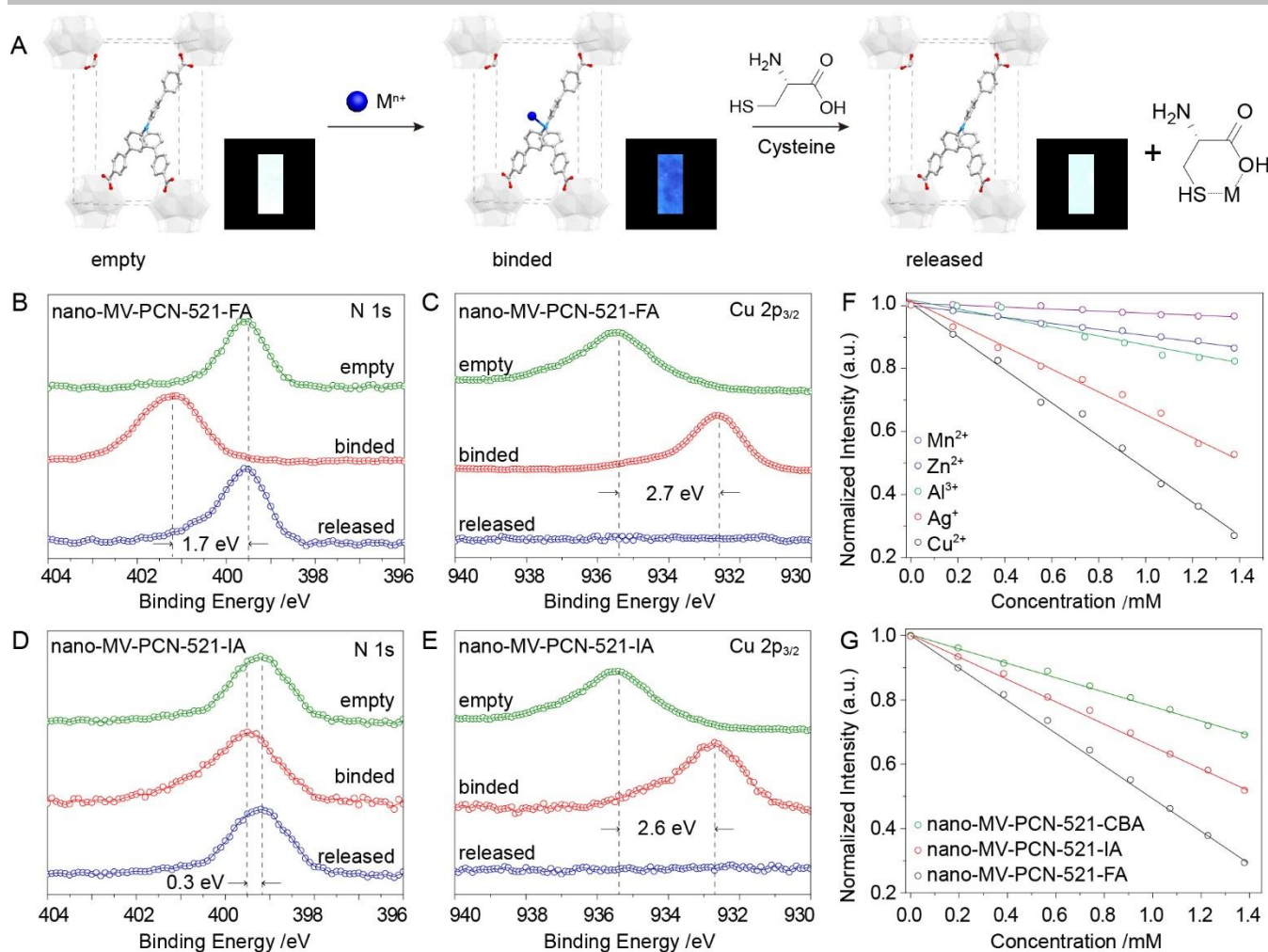


Figure 3. (A) Association and dissociation of metals in MV-PCN-521-FA, and fluorescence quenching and recovery displayed in test papers composed of nano-MV-PCN-521-FA. (B) N spectra and (C) Cu spectra in XPS analysis of nano-MV-PCN-521-FA, quenched by Cu^{2+} and recovered by cysteine. (D) N spectra and (E) Cu spectra in XPS analysis of nano-MV-PCN-521-IA, quenched by Cu^{2+} and recovered by cysteine. (F) Fluorescence intensity decrease in MV-PCN-521-FA versus the concentration of M^{n+} . (G) Fluorescence intensity decrease in MV-PCN-521-R versus the concentration of Cu^{2+} .

$2p_{3/2}$ peak shifted by 2.7 eV once anchored in this metal-binding site, while a shift of 2.6 eV was observed in that of nano-MV-PCN-521-IA with a different functional group. The difference in the shift of N 1s peak between these two nano-MV-MOFs was larger, 1.7 eV in the spectrum of nano-MV-PCN-521-FA, and 0.3 eV in that of nano-MV-PCN-521-IA, which can be attributed to better coordination of Cu^{2+} at the metal-binding sites in nano-MV-PCN-521-FA crystals (Table S8 and S9, Figure S96 and S108, SI). Although all kinds of metals can quench the fluorescence to some extent, the differences in their binding affinity was obvious (observed binding constants, K_{obs} varies from 1.56×10^2 to 1.70×10^4 , Figure 3F and 3G). The detailed coordination behavior of different metals in different metal-binding sites of MV-MOFs was described in Section S10 in SI.

Given the excellent affinity between Cu^{2+} and nano-MV-PCN-521-IA, a test paper composed of nano-MV-PCN-521-IA was prepared for the detection of biomarkers such as cysteine, homocysteine and glutathione, which are important health index.¹⁰ The fluorescence of the test paper was quenched by Cu^{2+} prior to the test, and immediately “turned-on”, when a solution of biomarkers was dripped on this test paper (Figure 3A and S83, SI). The concentration of biomarkers can be directly read from the intensity of the fluorescence in comparison to a standard titration curve (Figure S125 and S128, SI), with

extremely low detection limit, 22.5 nM and 46.4 nM, for L-cysteine and glutathione, respectively. It is worth noting that the detection of these thiol-molecules was not affected by the presence of urine, making these papers suitable for direct and quick test in physical examinations. They can be recycled for at least four times without losing their performance (Figure S83, SI). Given the excellent stability of these MV-MOFs in water, the corresponding test papers are well-suited for transport and storage in remote areas and countries lack of sophisticated medical instruments.

Acknowledgements

LSCM were performed in College of Life Science of Wuhan University with the assistance of Prof. M. Tang. SSNMR were collected at Wuhan Institute of Physics and Mathematics (WIPM), Chinese Academy of Sciences, with the assistance of Prof. J. Xu. We thank Prof. J. Xu (WIPM), Prof. M. Tang, Prof. H. Cong, Prof. F. Ke, C. Wang, X. Xu, C. Lei, X. Gong, X. Cai, H. Dai, Q. Han, X. He and W. Yan (Wuhan University) for their invaluable assistance and discussion. Financial support was provided by the 1000 Talent Plan of China, National Natural Science Foundation of China (21471118, 91545205, 91622103)

and National Key Basic Research Program of China (2014CB239203). Crystallographic data for the reported crystal structures have been deposited at the Cambridge Crystallographic Data Centre via www.ccdc.cam.ac.uk with codes 1585049, 1823238 and 1823239.

Conflict of interest

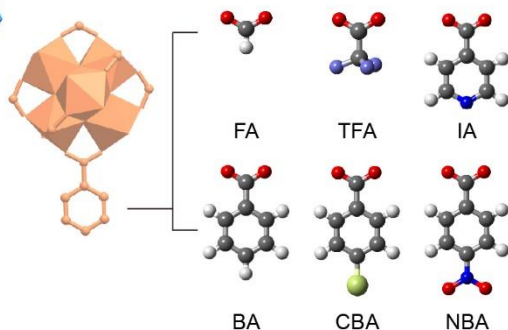
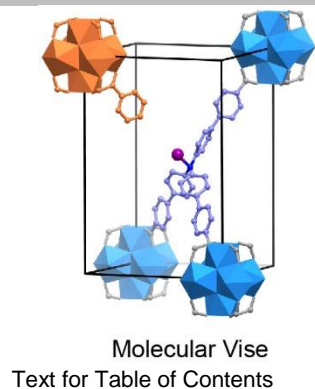
The authors declare no conflict of interest.

Keywords: coordination geometry • LSCM • metalation • metal-organic frameworks • turn-on sensor for biomarker

- (a) S. T. Zheng, T. Wu, C. Chou, A. Fuhr, P. Feng, X. Bu, *J. Am. Chem. Soc.* **2012**, *134*, 4517-4520. (b) F. Schröder, D. Esken, M. Cokoja, M. W. van den Berg, O. I. Lebedev, G. Van Tendeloo, B. Walaszek, G. Buntkowsky, H. H. Limbach, B. Chaudret, R. A. Fischer, *J. Am. Chem. Soc.* **2008**, *130*, 6119-6130. (c) S. Yuan, Y. P. Chen, J. Qin, W. Lu, X. Wang, Q. Zhang, H. C. Zhou, *Angew. Chem. Int. Ed.* **2015**, *54*, 14696-14700. (d) P. Ji, K. Manna, Z. Lin, X. Feng, A. Urban, Y. Song, W. Lin, *J. Am. Chem. Soc.* **2017**, *139*, 7004-7011. (e) A. E. Platero-Prats, A. B. League, V. Bernales, J. Ye, L. C. Gallington, A. Vjunov, A. J. Stevens, K. Chapman, *J. Am. Chem. Soc.* **2017**, *139*, 10410-10418. (f) M. H. Beyzavi, N. A. Vermeulen, A. J. Howarth, S. Tussupbayev, A. B. League, N. M. Schweitzer, J. Hupp, O. Farha, *J. Am. Chem. Soc.* **2015**, *137*, 13624-13631. (g) A. Cadiau, Y. Belmabkhout, A. Karim, P. M. Bhatt, R. S. Pillai, A. Shkurenko, C. Martineau-Corcoss, G. Maurin, M. Eddaoudi, *Science* **2017**, *356*, 731-735. (h) A. Cadiau, K. Adil, P. M. Bhatt, Y. Belmabkhout, M. Eddaoudi, *Science* **2016**, *353*, 137-140. (k) X. Cui, K. Chen, H. Xing, Q. Yang, R. Krishna, Z. Bao, H. Wu, W. Zhou, X. Dong, Y. Han, B. Li, Q. Ren, M. J. Zaworotko, B. Chen, *Science* **2016**, *353*, 141-144.
- (a) C. J. Doonan, W. Morris, H. Furukawa, O. M. Yaghi, *J. Am. Chem. Soc.* **2009**, *131*, 9492-9493. (b) Z. Wang, S. M. Cohen, *J. Am. Chem. Soc.* **2009**, *131*, 16675-16677. (c) A. M. Shultz, A. A. Sarjeant, O. K. Farha, J. T. Hupp, S. T. Nguyen, *J. Am. Chem. Soc.* **2011**, *133*, 13252-13255. (d) K. Manna, T. Zhang, W. Lin, *J. Am. Chem. Soc.* **2014**, *136*, 6566-6569. (e) H. Fei, S. M. Cohen, *J. Am. Chem. Soc.* **2015**, *137*, 2191-2194. (f) J. D. Evans, C. J. Sumbly, C. J. Doonan, *Chem. Soc. Rev.* **2014**, *43*, 5933-5951. (g) Q. G. Zhai, X. Bu, C. Mao, X. Zhao, L. Daemen, Y. Cheng, P. Feng, *Nature Commun.* **2016**, *7*, 13645. (h) J. Canivet, S. Aguado, Y. Schuurman, D. Farrusseng, *J. Am. Chem. Soc.* **2013**, *135*, 4195-4198. (i) B. Tu, Q. Pang, E. Ning, W. Yan, Y. Qi, D. Wu, Q. Li, *J. Am. Chem. Soc.* **2015**, *137*, 13456-13459.
- M. Zhang, Y. P. Chen, M. Bosch, T. Gentle, K. Wang, D. Feng, H. C. Zhou, *Angew. Chem. Int. Ed.* **2014**, *126*, 834-837.
- H. Wu, Y. S. Chua, V. Krungleviciute, M. Tyagi, P. Chen, T. Yildirim, W. Zhou, *J. Am. Chem. Soc.* **2013**, *135*, 10525-10532.
- (a) K. Koh, A. G. Wong-Foy, A. J. Matzger, *Angew. Chem. Int. Ed.* **2008**, *47*, 677-680. (b) H. Deng, C. J. Doonan, H. Furukawa, R. B. Ferreira, J. Towne, C. B. Knobler, O. M. Yaghi, *Science* **2010**, *327*, 846-850. (c) M. Kim, J. F. Cahill, H. Fei, K. A. Prather, S. M. Cohen, *J. Am. Chem. Soc.* **2012**, *134*, 18082-18088. (d) L. Liu, S. G. Telfer, *J. Am. Chem. Soc.* **2015**, *137*, 3901-3909. (e) C. Wang, K. E. DeKrafft, W. Lin, *J. Am. Chem. Soc.* **2012**, *134*, 7211-7124. (f) S. Yuan, Y. P. Chen, J. S. Qin, W. Lu, L. Zou, Q. Zhang, H. C. Zhou, *J. Am. Chem. Soc.* **2016**, *138*, 8912-8919. (g) L. Liu, T. Y. Zhou, S. G. Telfer, *J. Am. Chem. Soc.* **2017**, *139*, 13936-13943. (h) Z. Dong, Y. Sun, J. Chu, X. Zhang, H. Deng, *J. Am. Chem. Soc.* **2017**, *139*, 14209-14216. (i) N. Klein, I. Senkovska, I. A. Baburin, R. Gruenker, U. Stoeck, M. Schlichtenmayer, B. Streppel, U. Mueller, S. Leoni, M. Hirscher, S. Kaskel, *Chem. Eur. J.* **2011**, *17*, 13007-13016.
- (a) X. Kong, H. Deng, F. Yan, J. Kim, J. A. Swisher, B. Smit, O. M. Yaghi, J. A. Reimer, *Science* **2013**, *341*, 882-885. (b) L. J. Wang, H. Deng, H. Furukawa, F. Gándara, K. E. Cordova, D. Peri, O. M. Yaghi, *Inorg. Chem.* **2014**, *53*, 5881-5883. (c) Q. Liu, H. Cong, H. Deng, *J. Am. Chem. Soc.* **2016**, *138*, 13822-13825. (d) C. Castillo-Blás, A. Víctor, I. Puente-Orench, J. R. de Paz, R. Sáez-Puche, E. Gutiérrez-Puebla, F. Gándara, Á. Monge, *Sci. Adv.* **2017**, *3*, e1700773.
- (a) F. Persson, P. Bingen, T. Staudt, J. Engelhardt, J. O. Tegenfeldt, S. W. Hell, *Angew. Chem. Int. Ed.* **2011**, *50*, 5581-5583. (b) T. A. Planchon, L. Gao, D. E. Milkie, M. W. Davidson, J. A. Galbraith, C. G. Galbraith, E. Betzig, *Nat. Methods* **2011**, *8*, 417-423. (c) R. H. Webb, *Rep. Prog. Phys.* **1996**, *59*, 427-471. (d) W. R. Zipfel, R. M. Williams, W. W. Webb, *Nat. Biotechnol.* **2003**, *21*, 1369-1377.
- (a) H. Cheng, W. J. Lederer, M. B. Cannell, *Science* **1993**, *262*, 740-744. (b) F. S. Liao, W. S. Lo, Y. S. Hsu, C. C. Wu, S. C. Wang, F. K. Shieh, C. K. Tsung, *J. Am. Chem. Soc.* **2017**, *139*, 6530-6533.
- (a) N. Kitajima, K. Fujisawa, C. Fujimoto, Y. Morooka, S. Hashimoto, T. Kitagawa, A. Nakamura, *J. Am. Chem. Soc.* **1992**, *114*, 1277-1291. (b) H. S. Jung, P. S. Kwon, J. W. Lee, J. I. Kim, C. S. Hong, J. W. Kim, J. S. Kim, *J. Am. Chem. Soc.* **2009**, *131*, 2008-2012.
- (a) B. Wang, X. L. Lv, D. Feng, L. H. Xie, J. Zhang, M. Li, Y. Xie, J.-R. Li, H. C. Zhou, *J. Am. Chem. Soc.* **2016**, *138*, 6204-6216. (b) Y. Guo, X. Feng, T. Han, S. Wang, Z. Lin, Y. Dong, B. Wang, *J. Am. Chem. Soc.* **2014**, *136*, 15485-15488. (c) Y. Cui, Y. Yue, G. Qian, B. Chen, *Chem. Rev.* **2012**, *112*, 1126-1162.

Entry for the Table of Contents (Please choose one layout)

COMMUNICATION



Author(s), Corresponding Author(s)*

Page No. – Page No.

Title

Accepted Manuscript